Contents lists available at Science-Gate

International Journal of Advanced and Applied Sciences

Journal homepage: http://www.science-gate.com/IJAAS.html

Power splitters and feeding networks for PSR antenna array

Tomas Shejbal *, Tomas Zalabsky, Pavel Bezousek

Faculty of Electrical Engineering and Informatics, University of Pardubice, Pardubice, Czech Republic

ARTICLE INFO

Article history:
Received 27 December 2015
Received in revised form
24 January 2016
Accepted 27 January 2016

Keywords:
Antenna array
Distribution network
Monopulse secondary surveillance
Radar
Power divider
Primary surveillance radar
Radiation pattern synthesis

ABSTRACT

This paper deals with integrated antenna arrays combining a 3D primary surveillance radar (PSR) with a monopulse secondary surveillance radar (MSSR). The antenna arrays integration is briefly described. The synthesis methods of a cosecant squared vertical radiation pattern are investigated more deeply. Two synthesis methods are discussed: a Fourier synthesis and a phase synthesis. The description of different homogenous lines is presented and design of procedure of each distribution networks which consist of many power dividers is described. The measurement results of each manifold and methods of corrections are also presented and discussed.

1. Introduction

The design of radars for Air Traffic Control (ATC) has a long tradition in the Czech Republic. Mainly Primary Surveillance Radars (PSR) in S band, Precise Approach Radars (PAR) and Secondary Surveillance Radars (SSR) were built and supplied to many countries all over the world (Schejbal et al., 1994; Bezousek and Schejbal, 2004).

The primary and the secondary surveillance radars are frequently situated at the airport at one stand close to each other. Then it is advantageous to have the both radars integrated in one device with antennas collocated at the same turntable. During the past couple of years, the secondary radar antennas of such systems were located over the primary radar ones on the same pivots. In modern applications, secondary radars with sufficient earth reflection suppression, using large vertical SSR antenna apertures (Barton, 1988), are prevalent. It enlarges the total vertical dimension of the antenna system structure in described configuration and complicates the radar transportation mainly in the case of military applications. Integrated PSR/SSR reflector antennas occasionally emerged (Bezousek and Schejbal, 2004) but with no substantial spread due to inevitably compromised parameters.

Here we deal with a novel design of an antenna array, combining 3D primary surveillance radar antenna and monopulse secondary surveillance radar. This topology has an advantage in better mobility, lower height and better sufficient earth reflection suppression because of a high SSR aperture. The integration of the both antennas laid serious demands on the design and construction of the elements of the individual antennas.

The primary antenna, working in the S band (2.7 – 2.9 GHz) consists of 32 horizontal slotted waveguide rows each containing 75 radiating slots. Each waveguide is equipped with its own transmitter/receiver module and forms the same horizontal diagram. The transmitted signal covers all the elevation range at once through the favored cosecant vertical diagram. The bundle of the received beams is created beyond the receivers. The residual vertical polarization component of the irradiated field is suppressed by pairs of conductive vertical diaphragms between individual slots and forming vertical fins (see Fig. 1).

The described research was supported by the Internal Grant Agency of University of Pardubice, the project No. SGSFEI_2015004.

The L band (1.03 – 1.09 GHz) secondary radar antenna is made up of 27 identical antenna columns each containing a vertical feeder and eight radiators, creating the same vertical antenna pattern. The feeders are closed in the mentioned vertical fins of the primary antenna. The SSR antenna columns are fed by a horizontal feeder, creating the three standard horizontal beams: the sum, the difference and the control beam of the secondary radar. The design of the whole integrated antenna in more details is described in (Bezousek, 2014).

* Corresponding Author.
Email Address: tomas.shejbal@student.upce.cz (T. Shejbal)

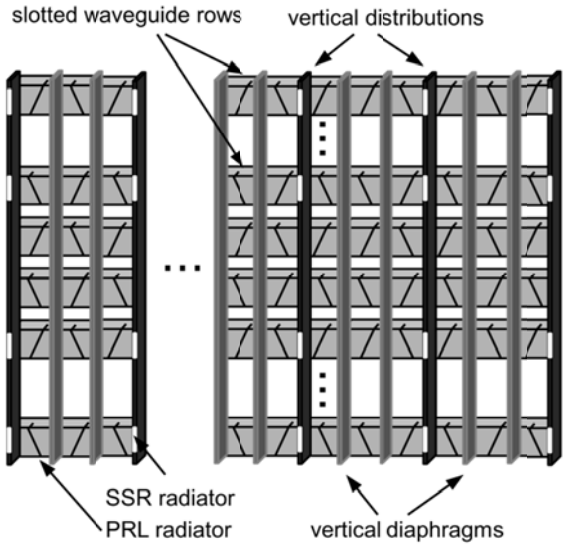

Fig. 1: The integrated PSR/SSR antenna design

2. Synthesis of the vertical radiation pattern

The ideal vertical radiation pattern of a PSR antenna array is a cosecant shaped pattern at seeking angles without side lobes outside an interval angle. The requirement is to have a wide radiation pattern in the vertical axis with cosecant shape from -1° to 45° with maximum around 7. This type of synthesis could be solved by many different synthesis methods, e.g.: Woodward-Lawson, Fourier synthesis, or phase synthesis (Balanis, 2011), (Oliner et al., 2007; Hansen, 2009; Shejbal, 2014). In this paper we deal with the second and third synthesis method.

2.1. Fourier synthesis

In the case of a Fourier synthesis method the ideal pattern (ideal radiated intensity of electric field) is straight forwardly used for computation of the Fourier transform (equation 2). The obtained amplitude and phase weights could be used for computation of the radiated intensity of an electric field (equation 1).

Equation 1 and 2 show the forward and the backward Fourier transform for a continuous linear aperture. In the case of discrete linear arrays integrals are substituted by summations and the exact point at aperture y is replaced by an inter-element spacing.

$$E(\Phi) = \int_{-\frac{D}{2}}^{\frac{D}{2}} A(y) e^{j\Psi(y)} e^{j2\pi\frac{y}{\lambda}\sin\Phi} \tag{1}$$

$$A(y)e^{j\Psi(y)} = \int_{-\pi}^{\pi} \left[E(\Phi) e^{-j2\pi\frac{y}{\lambda}\sin\Phi} \cos\Phi \right] d\Phi \tag{2}$$

Where: $E(\Phi)$ - ideal intensity of electric field,
D - Size of aperture,
$A(y)$ - amplitude weights,
$\Psi(y)$ - phase weights,
Φ - Azimuth,
y - Point at continuous aperture,
λ - Wavelength.

The Fourier transform is defined on a nonfinite interval. Because of that, the obtained pattern is only approximation to the ideal radiation pattern (as seen in Fig. 2).

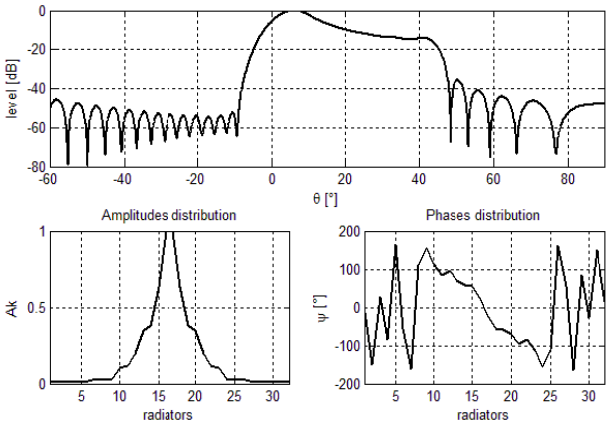

Fig. 2: The Fourier synthesis; top: array factor computed from computed amplitude and phase weights by Fourier synthesis; bottom left: amplitude weights; bottom right: phase weights (Shejbal, 2014)

Fig. 2 shows an array factor computed from amplitude and phase weights which are obtained by the Fourier transform method. The curve at angle interval from -1 to 45° meets the squared cosecant. Outside of this angle region are side lobes with good side lobe level.

2.2. Phase synthesis

A phase synthesis is based on the geometric laws for reflector arrays. There is an assumed curved shape of the imaginary wave surface which is created by the reflector antenna. From a different distance between each antenna element to the imaginary wave surface, it is possible to compute phase weighs of each element by equation 3.

$$\Psi_n = -\frac{2\pi}{\lambda}\sum_{r=1}^{n} d(n)\sin(\Theta_n) \tag{3}$$

Where: Ψ_n - phase weight of nth element, $d(n)$ - distance of nth element from center of antenna array, r - Distance from imaginary aperture to antenna element, Θ_n- angle between the nth ray and the antenna array element (each ray from imaginary reflector are orthogonal to shape of the reflector).

Fig. 3 shows an array factor (upper part) obtained by the phase synthesis. There is also shown an array factor multiplied by directivity of the horn element. Phase coefficients are shown in Fig. 3 (bottom left). Amplitude distribution is at all ports equal.

The phase synthesis has a higher ripple compared to the Fourier synthesis. On the other hand, equal amplitude coefficients for all antenna elements are the best advantage of the phase synthesis. That means one type of the transmitter

block is possible to use without need to design several types of transmitters. The next advantages of using of one transmitter type (compare too many transmitter types) are: lower cost and better maintenance.

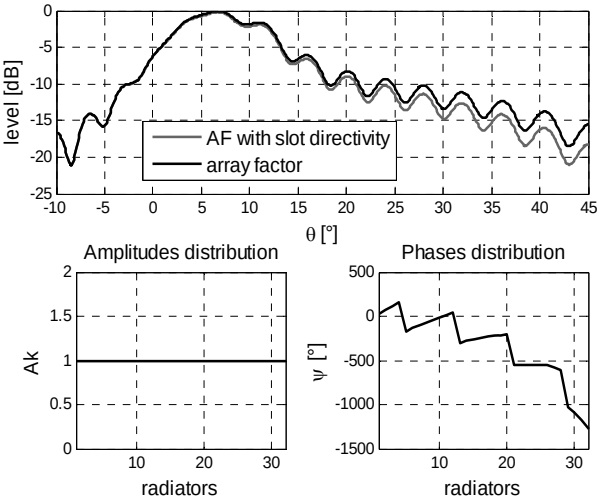

Fig. 3: The phase synthesis; top: array factor computed from determined amplitude and phase weights by the phase synthesis; bottom left: amplitude weights; bottom right: phase weights (Shejbal, 2014)

These reasons are why the phase synthesis amplitude and phase coefficients were chosen for next design of the transmitted signal distribution network. Phases of each output are listed in (Shejbal, 2014).

3. PSR antenna array feeders

Fig. 4 shows a flowchart of a PSR antenna (for better understanding of following description). The PSR antenna has 32 slotted waveguide rows with inter-element spacing 60 mm. Each horizontal waveguide row creates an identical horizontal radiation pattern (Chyba, 2013). All rows are fed by a transmitted signal manifold and form a vertical radiation pattern. Each horizontal array has its own receiver unit. Signals from the 1st and 2nd local oscillator are distributed to each receiver module by two independent distribution networks. These signals are used for down conversion of signals from a received frequency band to a lower frequency band, for next signal processing.

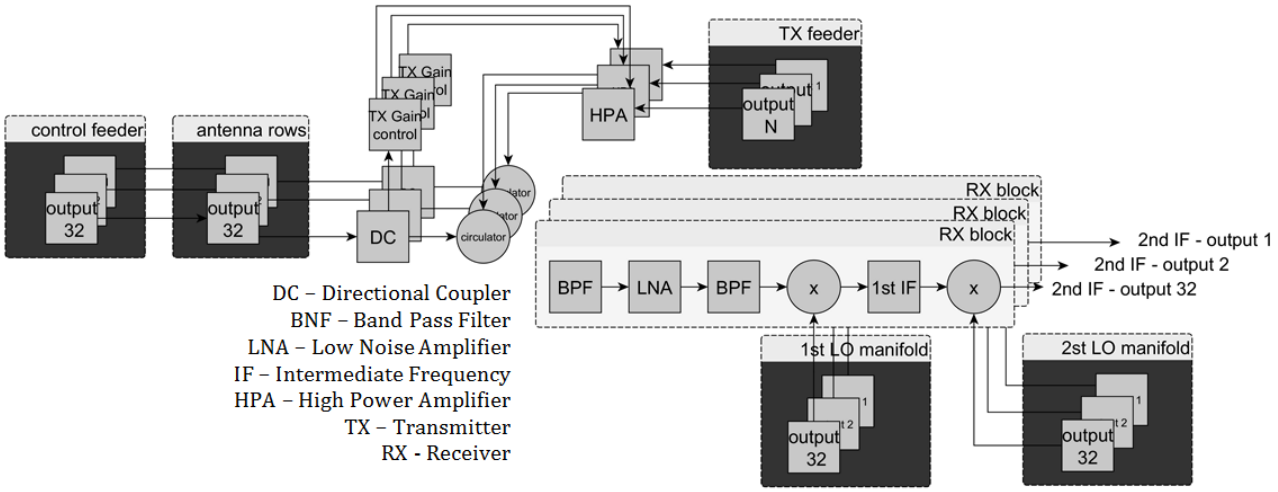

Fig. 4: The flowchart of PSR antenna array (each distribution is marked by dark grey color)

The last distribution network is used for calibrating of the antenna array. There is used loop with gain control of each transmitter unit for compensation of amplitude and phase deviations. Deviations are founded during the calibration process. The calibration process occurs in the blind zone (time between transmitting a pulse and echoes from near objects).

The requirements on each signal manifold are listed in Table 1.

Table 1: Required parameters for each manifolds.

signal manifold	bandwidth [GHz]	amplitude distribution	phase distribution
transmitted	2.7 – 2.9	equal	in 0(Shejbal, 2014)
control	2.7 – 2.9	equal	equal
1st LO	2.05 – 2.25	equal	equal
2nd LO	0.61	equal	equal

Because the equal amplitude weights and the number of horizontal rows (power of two) are considered, the equal power dividers could be used for the next design. The vertical distribution network scheme is shown in Fig. 6. The Wilkinson power dividers (Pozar, 2009) with equal signal splitting are used at each feeding network. Each signal manifold contains 31 power dividers.

3.1. Transmitted signal manifold

The demands on a transmitted distribution network are mainly low loss (because manifold is about 2 m long), electromagnetic compatibility, low height and simplicity of production. These demands lead to using of a both side suspended strip-line for transmitted manifold. The topology is shown in Fig. 5. There is substrate located in the middle of the structure between two conductive walls. The used material is FR4. There are copper strips from both sides of the substrate and both strips are conductively connected through many vias along the strips.

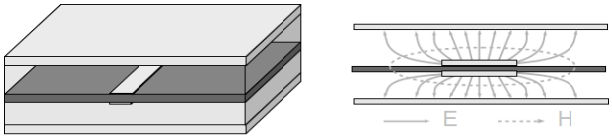

Fig. 5: The both side suspended strip-line: left: topology; right: cross section of strip-line with E and H fields (Shejbal, 2014)

Each power divider was, in the first design, computed from analytical formulas and after that solved in a 3D electromagnetic simulator – CST Microwave Studio (CST, 2015). The final designs are shown in the top part of the transmitted signal manifold shown in Fig. 7. The dividers consist of input strip-lines, quarter wavelength parts (circular quarter wave transformers) and output arms. Between the circular quarter-transformer is located a SMD resistor with resistance 100 Ω (only from one side).

The Wilkinson power dividers itself does not change the phase of the signal. It is done by trace extensions between individual dividers and outputs. Fig. 6 shows the scheme of a transmitted signal feeder. There are marked extensions (grey line) of each strip-line. The reference way is also marked. The phase delays between each output can be found in (Shejbal, 2014)0.

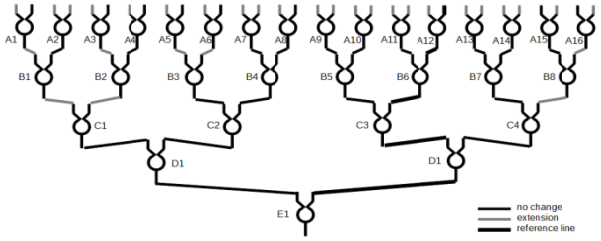

Fig. 6: The scheme of the transmitted signal manifold with marked extensions of the strip-line

The final distribution network design is shown in Fig. 7 (fabricated). Fig. 7shows strip-line meanders and other strip-line shapes (see outputs arms of each Wilkinson power divider) which do phase shift between the outputs.

3.2. Control signal manifold

The requirements are same as in the case of a transmitted signal feeder. The difference is in the (zero) phase shift between each port.

Due to these reasons, both side suspended strip-line technology and Wilkinson power dividers are used. The Wilkinson power dividers have same size and shape as the transmitted signal distribution. Because there is a requirement on zero phase shifts between each port, there are not any strip-line extensions between them.

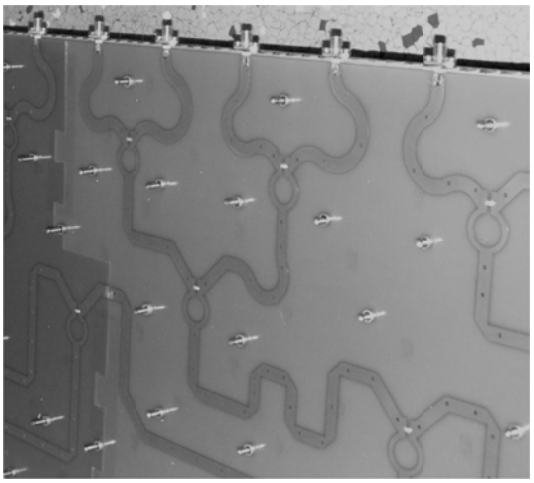

Fig. 7: The transmitted signal manifold during manufacturing

3.3. 1st local oscillator manifold

The requirement on amplitude and phase distribution is the same as in case of the control signal feeder. Again, the both side suspended strip-line is used and the Wilkinson power dividers are also used. The shape of power divider has a higher radius of quarter-wave transformer (due to lower frequency band) compared to previous dividers.

3.4. 2nd local oscillator manifold

The requirements on amplitude and phase distribution are again the same as in previous two cases. The strip-line cannot be used here due to the high dimensions of power dividers (one Wilkinson power divider should take space about 100 x 100 mm) and low inter-element spacing between outputs.

The first designs of dividers were on a microstrip line (shown in Fig. 8 during measurement of S-parameters; used vector analyzer is Rohde and Schwarz FSH4). The used substrate was FR4. After that, the design has changed to symmetric microstrip topology. That structure has higher electromagnetic compatibility and lower dimensions of dividers compare to a normal microstrip. The cross section of such topology is shown in Fig. 9. There are two microstrips structures. Both microstrips have separated ground planes. The used substrates are Rogers RO4003 with thickness of 1.524 mm. A common cooper strip is situated between them. The shape of dividers is similar to dividers shown in Fig. 8 with low reduction of dimensions due to higher relative permittivity.

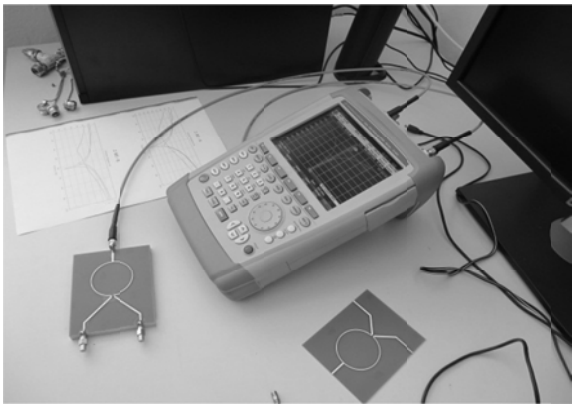

Fig. 8: The microstrip Wilkinson power divider during measurement of abs (S_{11}) parameter

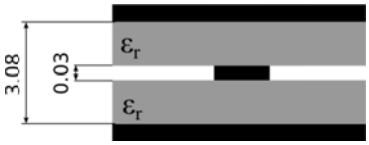

Fig. 9: Symmetric microstrip line structure

4. Results

The measurement of S-parameters has been done after the manufacturing process. The appropriate ports have been connected to vector analyzer Rohde and Schwarz FSH4 (FSH4, 2015) and the rest of the unused ports have been terminated by matched impedance. The absolute value of return loss at each port and isolation between adjacent ports has been measured. The complex signal transmission has been also measured at a frequency band which corresponds to a measured signal feeder.

From measured data standard deviations of absolute values of transmission and transmission phases are determined. The lower abs (S11) means the outputs are closer to equality of each port. In an ideal case the standard deviation is zero.

4.1. Transmitted signal manifold

The distribution network is designed for center frequency 2.8 GHz. One can see the lowest standard deviation of abs (S21) is in case of center frequency. In the bottom part of Table 2 phase deviations between computed and measured phases at each port are compared. Similar as in case of abs (S21), the lower standard deviation means better agreement between computed and measured phases. The corrections are done by extensions with coax cables of appropriate length. After application of corrections the standard deviation at center frequency is approximately 4 times lower that in the first design.

Fig. 10 shows comparison of three array factors. The black line is the synthetized array factor; the black dashed line is the array factor computed from the amplitude and the phase coefficients from the measurement. The last array factor is the array factor computed from new amplitude and phase coefficients. The new coefficients have been measured after application of phase corrections (by extensions with coax cables). The corrections have been done by coax cables with appropriate length. The array factor with those corrections is close to synthetized array factor (Table 2).

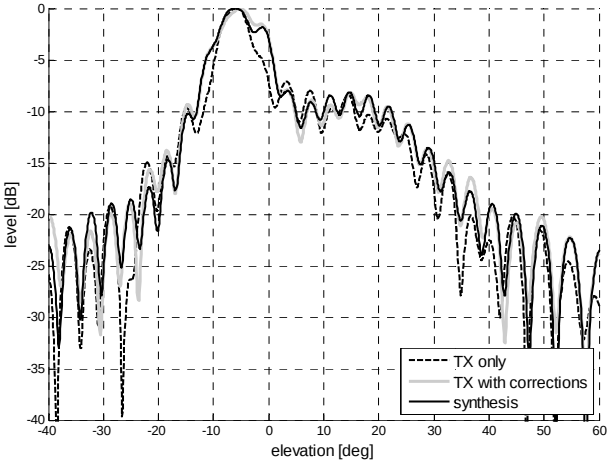

Fig. 10: The comparison of array factors computed from element phase differences for three cases: synthesis phases, measured phases without and with phase corrections

Table 2: Standard deviations of transmitted manifold outputs (computed from measured data at each output).

S21 standard deviations			
frequency [GHz]	2.7	2.8	2.9
amplitude [dB]	0.47	0.38	0.47
phse - first design [deg]	15.03	16.19	18.46
phase - with phase corrections [deg]	6.95	4.78	4.59

4.2. Control signal manifold

The amplitude and phase standard deviations are listed in Table 3. Deviations in magnitudes are low and they are the lowest at center frequency. Phase deviations are also acceptable.

Table 3: Standard deviations of control signal manifold outputs (computed from measured data at each output)

S21 standard deviations			
frequency [GHz]	2.7	2.8	2.9
amplitude [dB]	0.42	0.30	0.37
phase [deg]	3.67	3.12	2.64

4.3. 1st local oscillator manifold

The measurement of 1st LO manifold is again similar to previous distribution networks, with a difference in frequency band. Amplitude and phase deviations are listed in Table 4. The amplitude deviations are little higher compare to previous signal feeders, but still it is acceptable. Phase deviations are also acceptable, and for better performance phase corrections can be used in digital form (table with individual phase deviations can be add to signal processing).

4.4. 2nd local oscillator manifold

The measurement has been done by the same instrument with the same measuring procedure as in

previous manifolds; only the frequency band has been changed. The amplitude deviations are the lowest from all distribution networks and they are same for selected frequencies. The phase differences are close to each other at selected frequencies. Low phase deviations are able to compensate in digital form (similarly as in case of the 1st signal feeder).

Table 4: Standard deviations of 1st LO manifold outputs (computed from measured data at each output)

S21 standard deviations			
frequency [GHz]	2.05	2.15	2.25
amplitude [dB]	0.39	0.76	0.60
phase [deg]	9.51	5.99	5.52

Table 5: Standard deviations of 2nd LO manifold outputs (computed from measured data at each output)

S21 standard deviations			
frequency [MHz]	560	610	660
amplitude [dB]	0.06	0.06	0.06
phase [deg]	6.11	6.31	6.07

5. Conclusion

The integrated antennas of primary surveillance radar and monopulse secondary surveillance radar have been described. This topology has advantage in better mobility, lower height and better sufficient earth reflection suppression because of high SSR aperture. Two main synthesis methods have been discussed: the Fourier and the phase synthesis. The goal is to achieve sufficient radiation pattern with preservation of practical amplitude and phase distribution. It is important for further design of transmitted signal distribution networks. The design of the transmitted and the control signal distribution networks have been described. Design of signal feeders of the 1st and 2nd local oscillator has been also investigated. Each manifold consists of the same type of the power divider – Wilkinson power divider. A few photos of dividers and manifolds have been shown in the paper. The measurement of feeding networks has been described and results have been discussed. All manifolds are, after described corrections, mounted in PSR antenna array and these parts work suitably well.

References

Balanis CA (2011). Modern antenna handbook. John Wiley and Sons, New York, USA.

Barton DK (1988). Modern radar system analysis. Artech House, Norwood, USA.

Bezousek P and Schejbal V (2004). Radar technology in the Czech Republic. Aerospace and Electronic Systems Magazine, IEEE, 19(8): 27-34.

Bezousek P, Chyba M, Schejbal V, Karamazov S, Zalabsky T and Cernik L (2014). Combined antenna array for primary and secondary surveillance radars. In Antennas and Propagation in Wireless Communications (APWC), 2014 IEEE-APS Topical Conference on (pp. 597-600). IEEE.

Chyba M, Bezousek P, Pidanic J and Schejbal V (2013). Fan-beam array synthesis. In Antennas and Propagation (EuCAP), 2013 7th European Conference on (pp. 2165-2168). IEEE.

CST (2015). Available: https://www.cst.com [Accessed 24 July 2015].

FSH4 (2015). Available: https://www.rohde-schwarz.com/en/product/fsh-productstartpage_63493-8180.html [Accessed 24 July 2015].

Hansen RC (2009). Phased array antennas (Vol. 213). John Wiley and Sons, New York, USA.

Oliner AA, Jackson DR and Volakis JL (2007). Antenna engineering handbook. McGraw Hill, New York, USA.

Pozar DM (2009). Microwave engineering. John Wiley and Sons, New York, USA.

Schejbal V, Capalini R, Gotz J, Konecny J, Kupcak D, Kvitek E and Remta F (1994). Czech radar technology. Aerospace and Electronic Systems, IEEE Transactions on, 30(1): 2-17.

Shejbal T (2014). Signal manifolds for antenna array of a primary surveillance radar. Saarbrücken, Germany: LAP LAMBERT Academic Publishing, 2014. ISBN 978-3-659-66119-8.